coatings

MDPI

Article

The Influence of H Content on the Properties of a-C(W):H Coatings

Manuel Evaristo [1,*], Filipe Fernandes [1,2], Chris Jeynes [3] and Albano Cavaleiro [1,4]

[1] CEMMPRE–Centre for Mechanical Engineering Materials and Processes, Department of Mechanical Engineering, University of Coimbra Rua Luís Reis Santos, 3030-788 Coimbra, Portugal
[2] ISEP-School of Engineering, Polytechnic of Porto, Rua Dr. António Bernardino de Almeida 431, 4200-072 Porto, Portugal
[3] Ion Beam Centre, Advanced Technology Institute, University of Surrey, Guildford GU2 7XH, UK
[4] IPN-LED&MAT-Instituto Pedro Nunes, Laboratório de Ensaios, Desgaste e Materiais, Rua Pedro Nunes, 3030-199 Coimbra, Portugal
* Correspondence: manuel.evaristo@dem.uc.pt; Tel.: +351-239793745

Correspondence Table for the samples

In the supplementary material IBA report the samples with the numbers in the table corresponds to the samples used for the research work of the manuscript.

Reference number on the supplementary report	CH4 flow on the manuscript (sccm)
24	10
22	15
18	20
20	25
19	30
21	40

Samples and Purpose of Analysis

They are a selection of tribological DLC films on steel and on Si, unworn. We wish to determine the H content.

A Preliminary Report was with fits for a 3045 keV beam at normal incidence. The present Report completes the analysis for data (including ERD data) at glancing incidence and 4315 keV. The previous normal incidence analysis approximately determined the sample structure; this glancing incidence analysis crucially gives the H content (in the near-surface region) and also gives a direct signal for the surface C. This analysis starts from and includes the normal incidence 3 MeV analysis.

A second preliminary Report with (rough) fits for all the samples. In this analysis the data were fitted and then corrected using the misfit for the H signal for the correction factor. Manuel Evaristo responded with comments on samples ##18-24 (a set labelled "sample Coimbra"). This demonstrated that the method for correction was flawed and needed re-doing.

In this Report the "Coimbra" set of 7 samples is re-fitted in detail. For this set we can use a single structure file which must include oxygen since O is directly visible for all the samples. We also insist that the fits to the H signal are "good" and also that the general fits in the particle spectra for the other matrix elements are also "good" (not the case for Report2!).

Comments

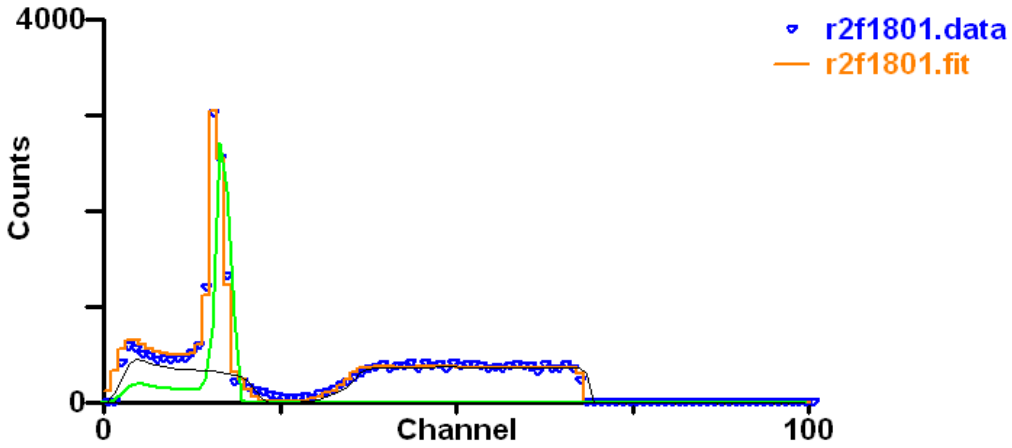

Sample#18: 4MeV (75° incidence, ~75° exit) small particle detector (172° scattering). Strongly non-Rutherford C signal is shown in green. The large particle detector has a similarly strong C signal. This strongly determines the C:W ratio in the films.

First the fits to the particle spectra are shown, with the PIXE fits following. There are 5 particle spectra, one for each of the backscattering detectors at both energies (4 spectra) and the ERD detector at the high energy. There are (usually) two PIXE spectra: one for each energy.

Then the H (ERD) fits are shown separately. This is really a repeat of the first data, but the H spectra are hard to see in the plots with 5 spectra (and fits). It can be seen that some of the fits are rather poor.

Then fitted profiles are shown for each sample. This is the basis of the report. Finding a structure that is reasonably consistent with the data is essential for interpreting the ERD spectra. **These profiles should be looked at carefully to see if they are feasible, given the existing knowledge of the samples, and whether they are credible.** They are determined only from the particle and X-ray data (assuming almost nothing about the samples: see below) and they contain a wealth of information. Some of this information may be useful, and some may be surprising. There is also further detailed information in the analysis which is not shown in the Report. Accessing this further information is easy in principle.

The ordinate for the fitted profiles is given in absolute thin film units: g/cm^2. This is because I do not have a reliable value for the densities of many of these materials. Given the density (g/cc), the linear thickness follows immediately.

The fits were all done *assuming* that each sample had H bound to C in a constant ratio. That is, the spectra for each sample were fitted with a *logical element* (a molecule!) CH_z where z was a fitting parameter. The fit displayed show that this is usually a good assumption, but some of the data is not consistent with this assumption. If necessary we can refit these spectra relaxing this very strong assumption imposed on the data.

Given a good fit to the H signal, the absolute (systematic) uncertainty is dominated by the ERD calibration accuracy, which I estimate as ~8%, see [1]. However, the fits to the H signal are not that good, and this is despite repeated fitting. The misfit factor is given in Table 1. A full multiparameter fit is being made on all seven spectra (five particle and 2 photon) and the fitting code is harmonising all the spectra. So, for example, in #18 the Cr layer thickness is fitted well by the B detector at normal incidence (spectrum#5) but apparently overestimated at tilted incidence (spectrum#2). I have not yet found the origin of these inconsistencies.

Table S1. Misfit factor for H signal.

Sample	Data/Fit
18	0.91
19	0.81
20	0.98
21	0.86
22	0.97
23	0.97
24	1.06

Conclusions

Results for the film stoichiometry (including H content) and thickness are summarised for the whole dataset in Table S2 (p.5).

The fits were all done *assuming* that each sample had H bound to C in a constant ratio. That is, the spectra for each sample were fitted with a *logical element* (a molecule!) CH_z where z was a fitting parameter. The fit displayed show that this is usually a good assumption, but some of the whole dataset is not consistent with this assumption, although these seven samples are reasonably consistent.

The H signal is clearly not always fitted well, and Table 1 shows the misfit factor. This must represent the fitting uncertainty in some way, but all the data should be taken together. Therefore the Table 2 results should be preferred, with Table 1 suggesting a possible 10% uncertainty on the fitting.

Analysis

For each sample, for the higher energy (4315 keV), only grazing beam incidence spectra were collected on four detectors (2 particle backscattering, one PIXE, one particle forward recoil for the H ERD signal). Normal incidence spectra were collected for the lower energy (3045 keV) on three detectors (2 particle backscattering, one PIXE). Thus there are (usually) seven spectra per sample.

The 3 MeV particle spectra have high sensitivity to O near the surface (through the $^{16}O(\quad)^{16}O$ resonance at 3038 keV) and the 4.3 MeV spectra have high sensitivity to C near the surface (through the $^{12}C(\quad)^{12}C$ resonance at 4260 keV). The films are quite thick, so the high energy is needed to see the H profile in most of the thickness.

NDFv9.4e (17th Jan 2012) was used to fit the data [2].

EBS (non-Rutherford) scattering cross-sections are taken from IBANDL (http://www-nds.iaea.org/ibandl/ and see [3].

SigmaCalc "http://www-nds.iaea.org/sigmacalc/" and [4] is used for evaluated cross-sections (H, C, N, O, Si etc). NDFv9.3e and above implements interpolation of tables derived from SigmaCalc.

SRIM 2003 [5] stopping powers were used. For PIXE only SRIM 2000 stopping was available.

The pulse pileup calculation in NDF uses either the algorithm of Wielopolski & Gardner [6] or that of Molodtsov & Gurbich The MG algorithm takes proper account of tail pileup without the parabolic pulse shape [7] approximation of the WG algorithm. It is significantly better in higher count rate applications where the pulse loss from large signals is significantly underestimated by WG.

The pulse height defect for the Si particle detectors was calculated using [8].

Roughness (layer thickness variation) was present in all these samples. This is fitted using the algorithm of Barradas [9].

EBS cross-sections

Results

(For experimental setup and detailed results and discussion, please refer to the Appendix).

Table S2. C/H ratio for all samples, from fitted data.

Sample	February Report			March Report												
	C(1-x) Hx fitted x %	C from fit TFU	H from data TFU	C(1-x) Hx fitted x %	C TFU	H TFU	W TFU	Ar TFU	O TFU	Cr TFU	C from fit at%	H from fit at%	W from fit at%	Ar from fit at%	O from fit at%	Fitted Film Thickness DLC:W mg/cm^2	Fitted Film Thickness Cr nm
18	28.0	8865	4309	30.4	8531	3726	566	132	198	2241	64.9%	28.3%	4.3%	1.00%	1.5%	0.363	269
19	31.2	8769	4804	32.4	8615	4129	465	27	170	2545	64.3%	30.8%	3.5%	0.20%	1.3%	0.327	306
20	37.5	7662	5296	30.8	8536	3799	527	59	116	2288	65.5%	29.1%	4.0%	0.45%	0.9%	0.344	275
21	36.5	8992	6525	31.9	9136	4279	406	5	201	2384	65.1%	30.5%	2.9%	0.04%	1.4%	0.319	286
22	34.0	6953	4003	28.8	8243	3334	576	187	194	2352	65.8%	26.6%	4.6%	1.50%	1.5%	0.363	282
23	37.5	9224	6997	32.8	9951	4857	303	5	597	2304	63.3%	30.9%	1.9%	0.03%	3.8%	0.315	277
24	19.3	8002	5147	28.7	7934	3194	609	191	169	2195	65.6%	26.4%	5.0%	1.58%	1.4%	0.366	264

APPENDIX

Depth Profiling by Ion Beam Analysis

This work was done using a 2MV Tandetron accelerator from High Voltage Engineering Europe, commissioned summer 2002 at the University of Surrey Ion Beam Centre. This machine is capable of generating proton beams up to 4MeV and alpha particle beams of up to 6MeV [10].

Rutherford backscattering spectrometry (RBS) is an accurate, powerful and general thin film depth profiling technique typically carried out with 2 MeV He beams. Higher energy and proton beams are typically used for depth profiling thicker films, and for enhancing sensitivity to light elements with non-Rutherford elastic backscattering (EBS). Hydrogen can be depth profiled using elastic forward recoil spectrometry (FRS, also known as ERD: elastic recoil detection). Deuterium can also be depth profiled using nuclear reaction analysis (NRA) with a ^{3}He beam. Particle induced X-ray emission (PIXE) has little depth resolution but can unambiguously identify elements and analyse for trace elements with detection limits approaching μg/g. Particle induced gamma-ray emission (PIGE) is a form of NRA particularly valuable for lighter elements present in bulk materials at a trace level: F, Na, Al, Si.

The depth profiling beamline is equipped with a 6-movement goniometer from Arun Microelectronics Ltd, commissioned autumn 2002. This instrument is capable of loading entire 100mm wafers through a load lock, of channelling in arbitrary directions on a single crystal, and of high depth resolution (glancing beam incidence geometry). Both backscattering and forward recoil detectors are fitted. The target chamber has a base vacuum below 1 nbar.

The microbeam beamline was commissioned summer 2002. It has a magnetic quadrupole triplet lens and associated equipment from Oxford Microbeams Ltd, and can focus the beam to about 1 micron. The beam can be scanned over about 2mm giving trace and minor element mapping with PIXE and 3D depth profiling with RBS/EBS using the OMDAC and DAN32 software [11] (which is based on the GUPIX code [12]. Various sample stages are available including a cold stage, a goniometer, and a stage suitable for ion beam induced current (IBIC).

The external beamline was commissioned May 2004 and also has a magnetic quadrupole triplet with a thin window so that a focussed and scanned ion beam can be passed into air to analyse large, delicate or wet samples by PIXE, RBS/EBS and PIGE.

Depth profiles can be extracted automatically from RBS, EBS, ERD and NRA spectra using the Surrey IBA DataFurnace software [13] (http://www.surreyibc.ac.uk/ndf). We have validated the accuracy of this code against a certified standard sample [14]. The code is also validated by an international intercomparison [15]. DataFurnace v9 [2], can also now handle PIXE data (with other IBA data) self-consistently [16] and more correctly than GUPIX.

Where the DataFurnace fit is *good* the fitted profile is *valid* (but not necessarily true!). In the analyses we will point out the limitations of the results due to counting statistics, finite energy and depth resolution, and other systematic errors. Profiles are always given as layer structures. We systematically use *Occam's Razor* ("minimise your assumptions") to be objective about how much information is really in the data: in particular the extracted layer structures tend to be as *coarse* as the data will allow, and the discontinuous profiles we always show are due to the finite energy and depth resolution of the technique and can be seen as an expression of these.

Complete data sets are archived and can be re-analysed on request. In particular, a rigorous statistical evaluation of the uncertainty of the depth profiles can be obtained with the Bayesian techniques natural to the DataFurnace implementation. We have an interest in accurate work with rigorous evaluation of uncertainties, and are always interested in joint publication.

Dr.Chris Jeynes, University of Surrey Ion Beam Centre Guildford, GU2 7XH
c.jeynes@surrey.ac.uk: www.surreyibc.ac.uk
tel: 01483 689829 (Mrs.Karen Arthur: 01483 686090) *July 2009*

Samples and Purpose of Analysis

Samples arrived 14th November 2011 with Manuel Evaristo. They are a selection of tribological DLC films on steel and on Si, unworn. We wish to determine the H content.

A Preliminary Report was sent 6th December 2011 with fits for a 3045 keV beam at normal incidence. The present Report completes the analysis for data (including ERD data) at glancing incidence and 4315 keV. The previous normal incidence analysis approximately determined the sample structure; this glancing incidence analysis crucially gives the H content (in the near-surface region) and also gives a direct signal for the surface C. This analysis starts from and includes the normal incidence 3 MeV analysis.

A second preliminary Report was sent 2nd February 2012 with (rough) fits for all the samples. In this analysis the data were fitted and then corrected using the misfit for the H signal for the correction factor. Manuel Evaristo responded with comments on samples ##18-24 (a set labelled "sample Coimbra"). This demonstrated that the method for correction was flawed and needed re-doing.

In this Report the "Coimbra" set of 7 samples is re-fitted in detail. For this set we can use a single structure file which must include oxygen since O is directly visible for all the samples. We also insist that the fits to the H signal are good and also that the general fits in the particle spectra for the other matrix elements are also good (not the case for Report2!).

Analytical Conditions

3.045 MeV $^{4}He^{+}$, 16th November 2011. The beam current was 1 - 8 nA, nominal beam size 1mm.

4315 keV $^{4}He^{++}$, 17th November 2011. The beam current was ~10 nA (5 pnA, particle nA, since beam is doubly charged) nominal beam size 1mm. At glancing incidence the footprint of the beam on the sample was ~4x1 mm. Some samples had to be oriented under the beam for the beam to fall squarely on the sample. For example, #32 had = 0° and #29 had = 117°. The goniometer had a Z stage (movement 5mm) to bring the eucentric point into the sample surface, but the goniometer alignment was not sufficiently precise to allow

completely automatic operation. For each sample the location of the beam was verified visually, using the beamline beam-location laser, adjusting manually as necessary.

Detector scattering angle 172.8º (RBS detector A, Cornell geometry), 148.6 (RBS detector B, IBM geometry), 30.75° (ERD detector C, IBM geometry), solid angles 1.2, 6.5, 1.25 msr for detectors A, B, C respectively.

The PIXE detector was at 60° to the beam, with a solid angle 1 msr and a 146 m Be filter.

Beam incident in a near-normal direction, and at glancing incidence (75°) for ERD (exit angles, A~75°, B~45°, C~75°). The ERD range foil was 32 m Kapton (4 * 8 m foils), that is, ($C_{22}H_{10}O_5N_2$) with 279135 TFU or 4.544 mg/cm^2 at 1.42g/cc.

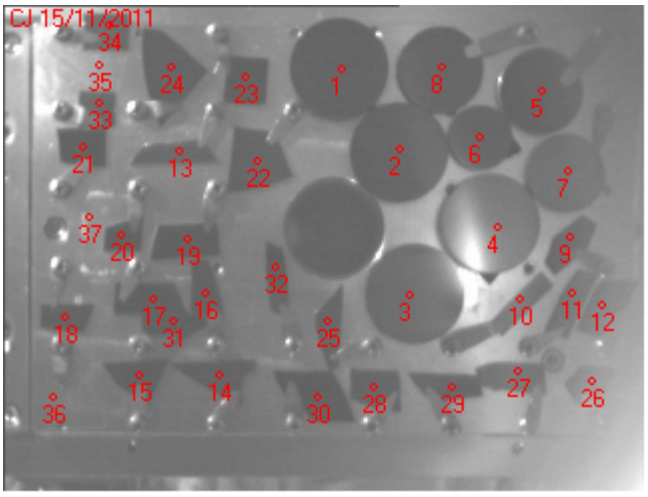

32 samples were loaded. Samples held by clips, except the large metals discs which were held by carbon tape. Samples ##33 & 34 are AuNiSiO$_2$/Si calibration samples, #35 is the kapton sample for calibrating ERD, and #36 is the glass for visualising the beam.

See Table 1 for the numbering of the samples.

Calibration

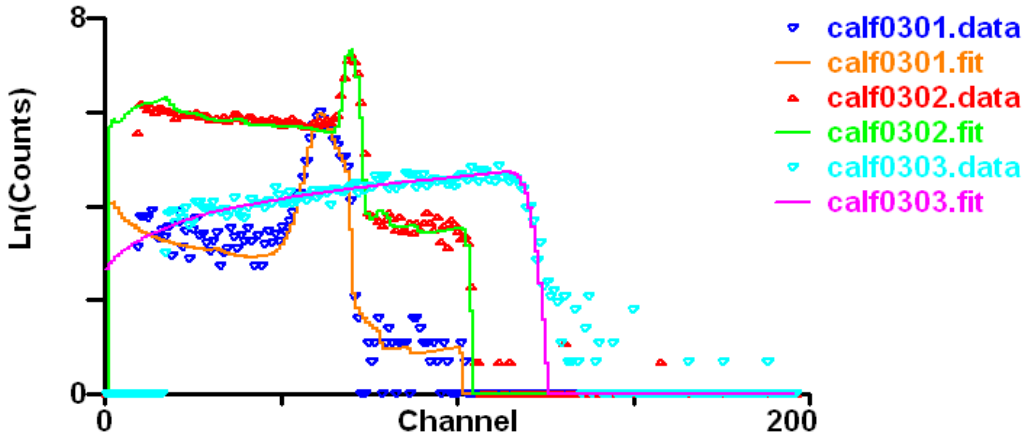

Scheme 22. $H_{10}O_5N_2$) at glancing incidence for all three detectors A, B, C at 4315 keV $^4He^{++}$. This determines the solid angle ratio C/A and C/B.

Note all of C, O, N, H are strongly non-Rutherford. Note also the pronounced resonance for C. The ERD signal is fitted using 260000 TFU foil equivalent thickness (determined from a previous analysis) and an appropriate amplifier gain to fix the keV/ch.

PIXE calibration the same as for Report#1.

Results: Fits of particle spectra

We give, for 7 of 32 samples, the plot of all the particle spectra fitted

Sample 1. Spectra##1,2 are A & B detectors, 4315 keV glancing incidence; Spectrum#3 is ERD detector, 4315 keV glancing incidence; Spectra##4,5 are A & B detectors, 3045 keV normal incidence. These are all fitted (together with the PIXE spectra) self-consistently.

Sample 2
Sample 3
Sample 4
Sample 5
Sample 6
Sample 7
Sample 8
Sample 9
Sample 10
Sample 11
Sample 12
Sample 13
Sample 14
Sample 15
Sample 16
Sample 17

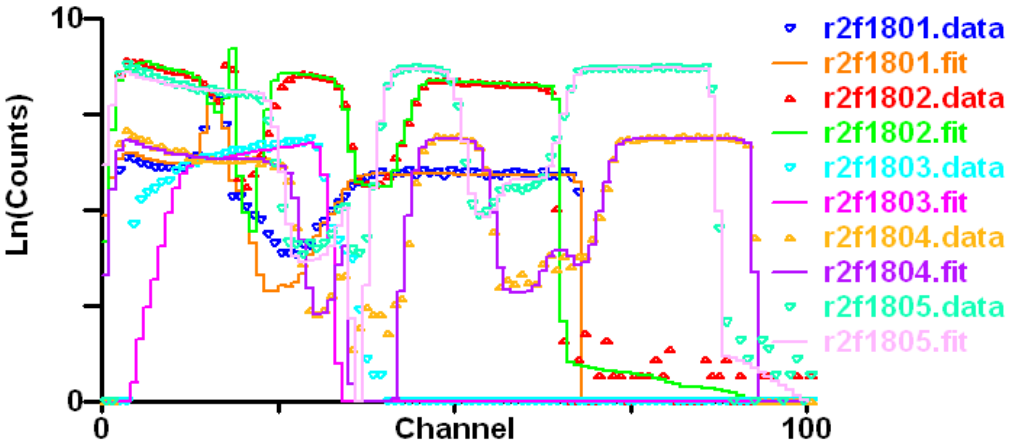

Sample 18

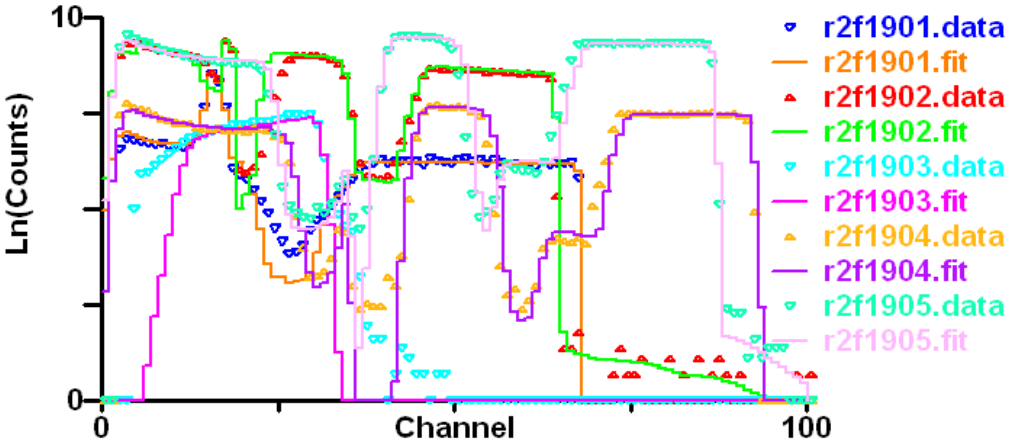

Sample 19

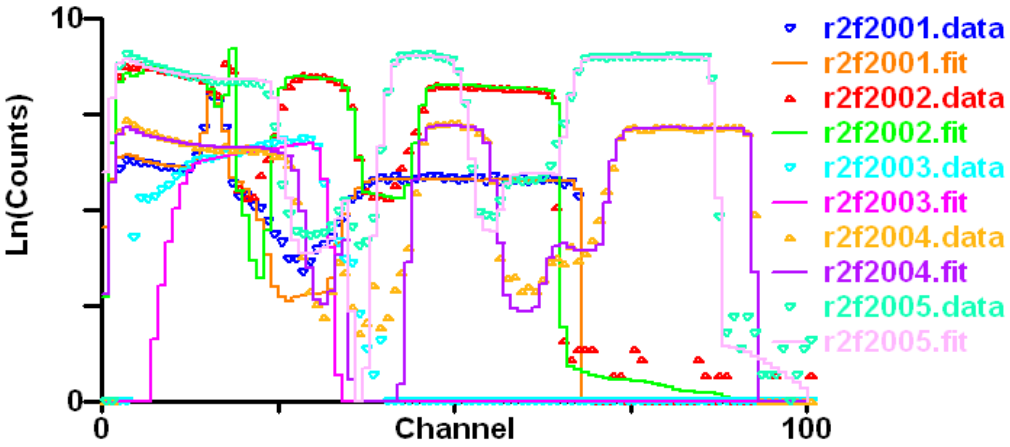

Sample 20

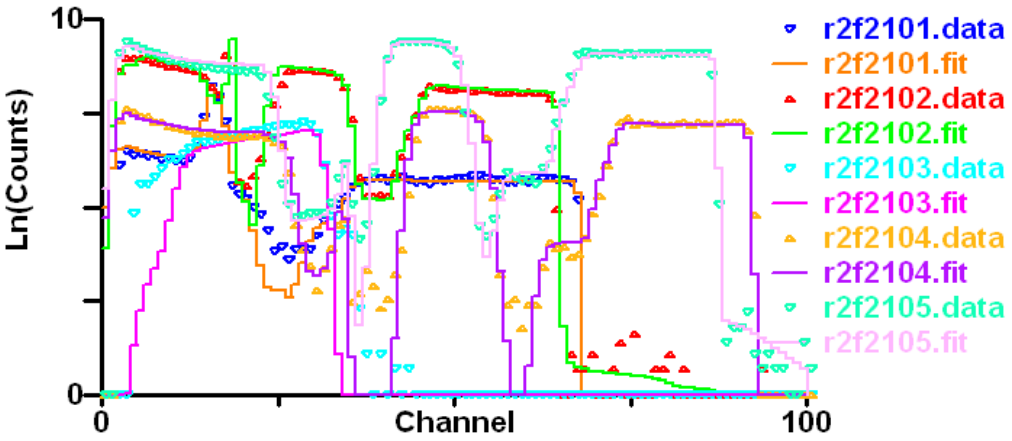

Sample 21

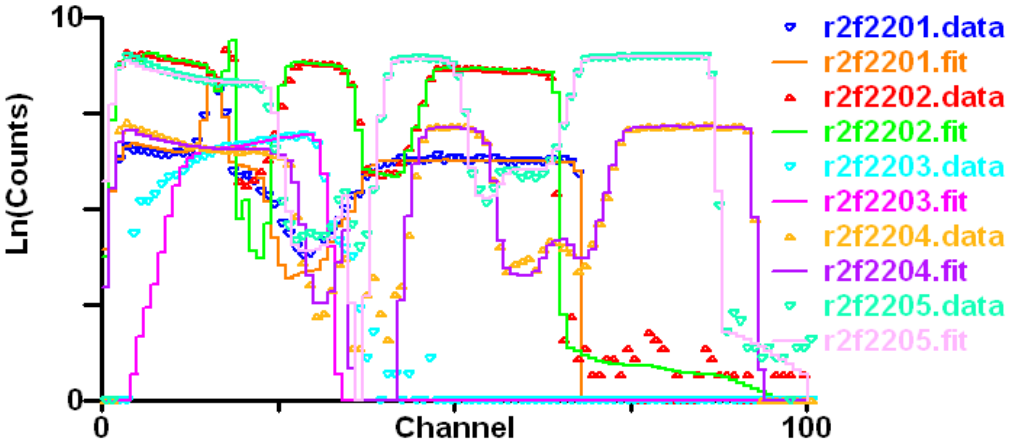

Sample 22

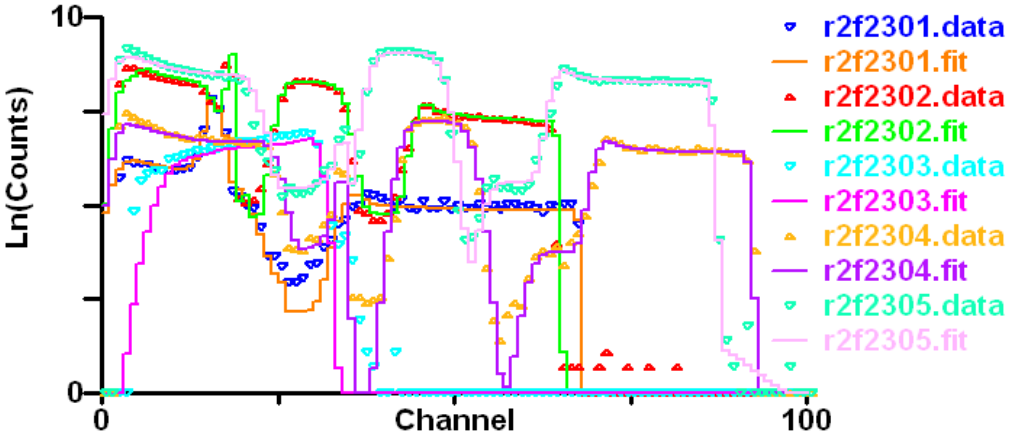

Sample 23

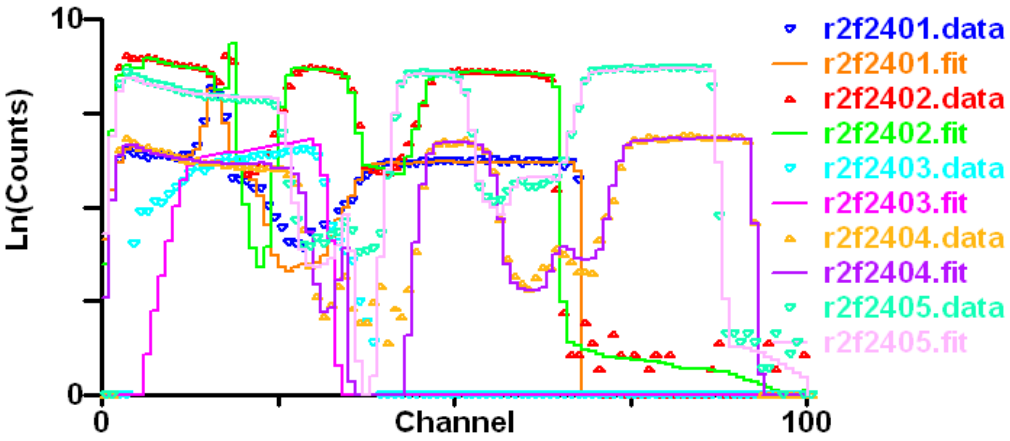

Sample 24
Sample 25
Sample 26
Sample 27
Sample 28
Sample 29
Sample 30
Sample 31
Sample 32

Results: PIXE fitsSample 1: 3 MeV normal incidence, 60° exit

Sample 1: 4 MeV glancing incidence, near-normal exit.
Sample 2: 3 MeV normal incidence, 60° exit
Sample 2: 4 MeV glancing incidence, near-normal exit.
Sample 3: 3 MeV normal incidence, 60° exit
Sample 4: 3 MeV normal incidence, 60° exit
Sample 4: 4 MeV glancing incidence, near-normal exit.
Sample 5: 3 MeV normal incidence, 60° exit
Sample 5: 4 MeV glancing incidence, near-normal exit.
Sample 6: 3 MeV normal incidence, 60° exit
Sample 6: 4 MeV glancing incidence, near-normal exit.
Sample 7: 3 MeV normal incidence, 60° exit
Sample 7: 4 MeV glancing incidence, near-normal exit.
Sample 8: 3 MeV normal incidence, 60° exit
Sample 8: 4 MeV glancing incidence, near-normal exit.
Sample 9: 3 MeV normal incidence, 60° exit
Sample 9: 4 MeV glancing incidence, near-normal exit.
Sample 10: 3 MeV normal incidence, 60° exit
Sample 10: 4 MeV glancing incidence, near-normal exit.
Sample 11: 3 MeV normal incidence, 60° exit
Sample 11: 4 MeV glancing incidence, near-normal exit.
Sample 12: 3 MeV normal incidence, 60° exit
Sample 13: 3 MeV normal incidence, 60° exit
Sample 13: 4 MeV glancing incidence, near-normal exit.
Sample 14: 3 MeV normal incidence, 60° exit
Sample 14: 4 MeV glancing incidence, near-normal exit.
Sample 15: 3 MeV normal incidence, 60° exit
Sample 15: 4 MeV glancing incidence, near-normal exit.
Sample 16: 3 MeV normal incidence, 60° exit

Sample 16: 4 MeV glancing incidence, near-normal exit.
Sample 17: 3 MeV normal incidence, 60° exit
Sample 17: 4 MeV glancing incidence, near-normal exit.

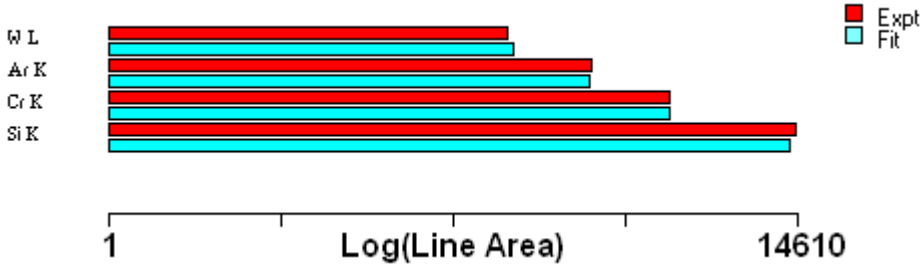

Sample 18: 3 MeV normal incidence, 60° exit

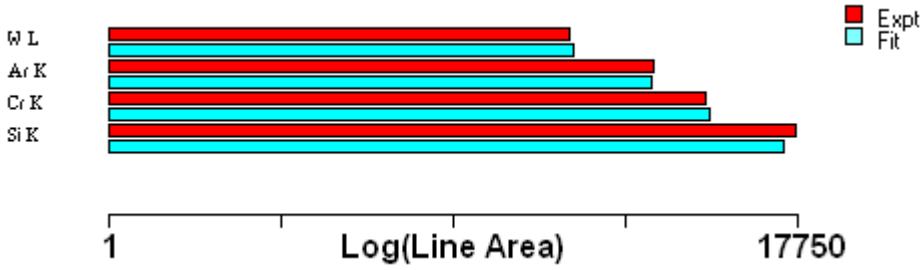

Sample 18: 4 MeV glancing incidence, near-normal exit.

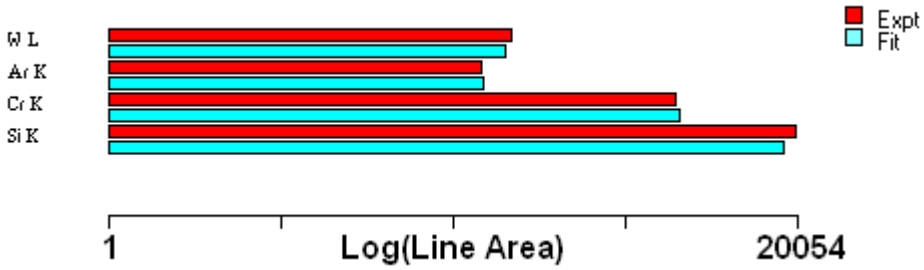

Sample 19: 3 MeV normal incidence, 60° exit

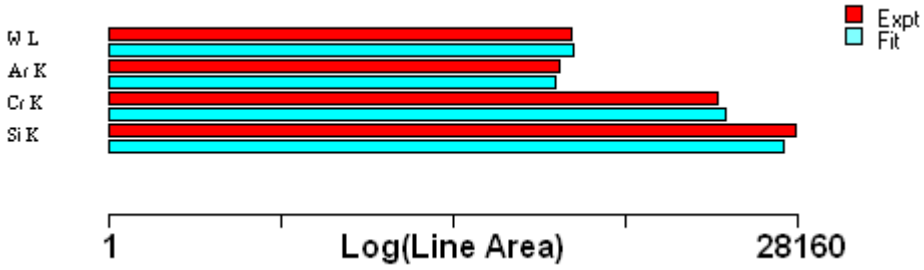

Sample 19: 4 MeV glancing incidence, near-normal exit.

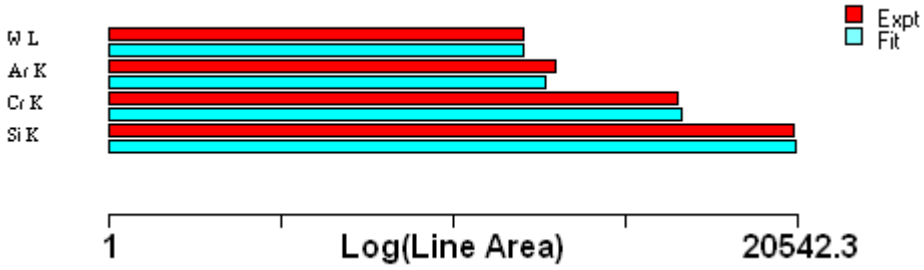

Sample 20: 3 MeV normal incidence, 60° exit

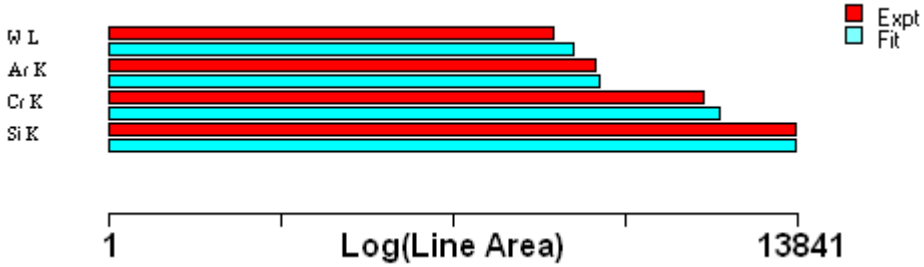

Sample 20: 4 MeV glancing incidence, near-normal exit.

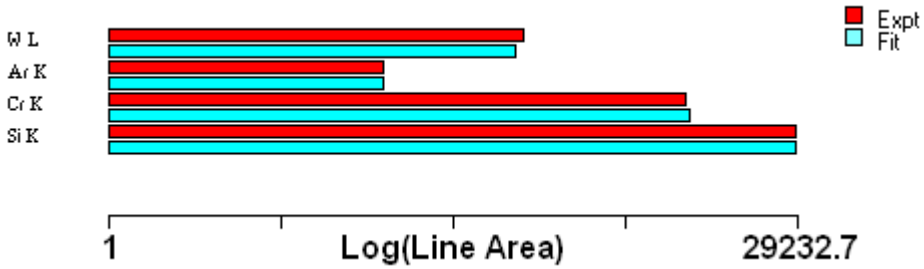

Sample 21: 3 MeV normal incidence, 60° exit

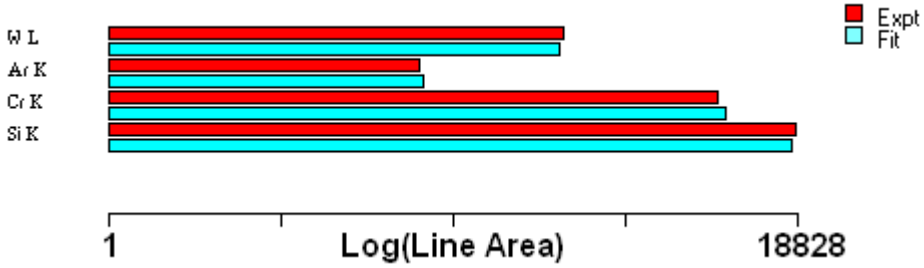

Sample 21: 4 MeV glancing incidence, near-normal exit.

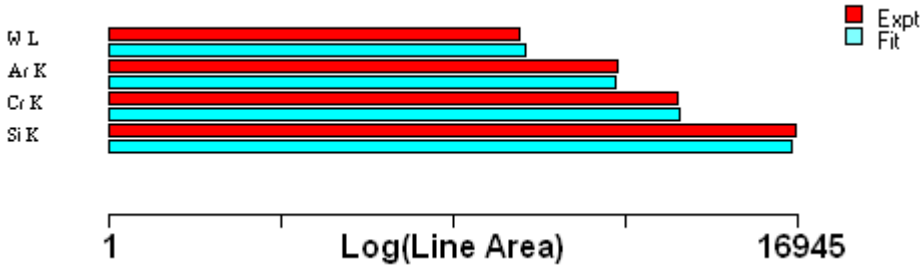

Sample 22: 3 MeV normal incidence, 60° exit

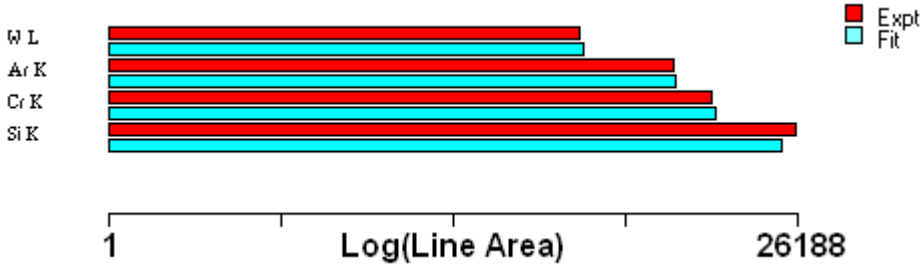

Sample 22: 4 MeV glancing incidence, near-normal exit.

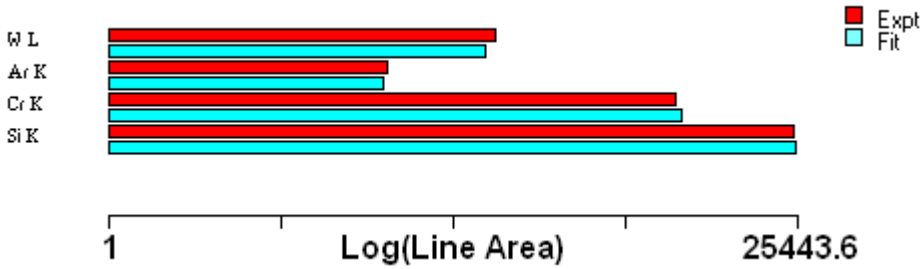

Sample 23: 3 MeV normal incidence, 60° exit

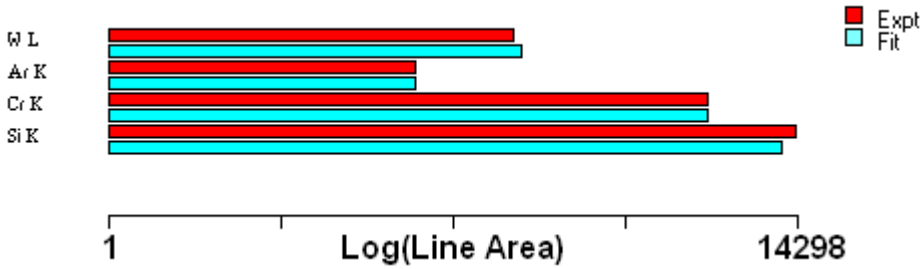

Sample 23: 4 MeV glancing incidence, near-normal exit.

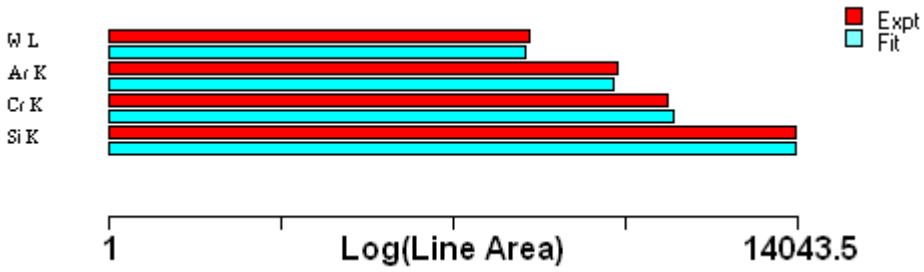

Sample 24: 3 MeV normal incidence, 60° exit

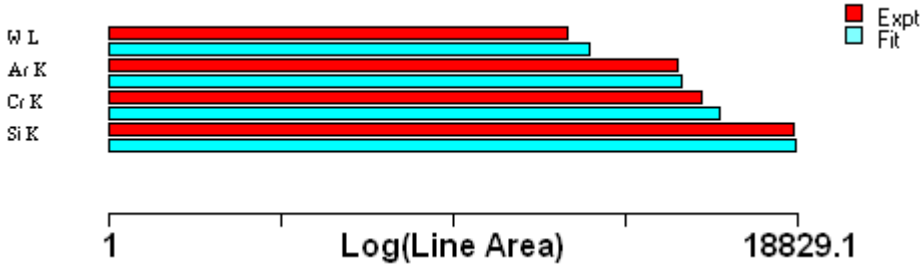

Sample 24: 4 MeV glancing incidence, near-normal exit.
Sample 25: 3 MeV normal incidence, 60° exit
Sample 25: 4 MeV glancing incidence, near-normal exit.
Sample 26: 3 MeV normal incidence, 60° exit
Sample 26: 4 MeV glancing incidence, near-normal exit.
Sample 27: 3 MeV normal incidence, 60° exit
Sample 27: 4 MeV glancing incidence, near-normal exit.
Sample 28: 3 MeV normal incidence, 60° exit
Sample 28: 4 MeV glancing incidence, near-normal exit.
Sample 29: 3 MeV normal incidence, 60° exit
Sample 29: 4 MeV glancing incidence, near-normal exit.
Sample 30: 3 MeV normal incidence, 60° exit
Sample 30: 4 MeV glancing incidence, near-normal exit.
Sample 31: 3 MeV normal incidence, 60° exit
Sample 32: 3 MeV normal incidence, 60° exit

Sample 1: ERD spectra (H signal) and fit. $C_{(1-x)}H_x$: x = 23%
Sample 2: ERD spectra (H signal) and fit. $C_{(1-x)}H_x$: x = 28%
Sample 3: ERD spectra (H signal) and fit. $C_{(1-x)}H_x$: x = 11%
Sample 4: ERD spectra (H signal) and fit. $C_{(1-x)}H_x$: x = 16%
Sample 5: ERD spectra (H signal) and fit. $C_{(1-x)}H_x$: x = 39%
Sample 6: ERD spectra (H signal) and fit. $C_{(1-x)}H_x$: x = 10%
Sample 7: ERD spectra (H signal) and fit. $C_{(1-x)}H_x$: x = 33%
Sample 8: ERD spectra (H signal) and fit. $C_{(1-x)}H_x$: x = 45%
Sample 9: ERD spectra (H signal) and fit. $C_{(1-x)}H_x$: x = 30%
Sample 10: ERD spectra (H signal) and fit. $C_{(1-x)}H_x$: x = 16%
Sample 11: ERD spectra (H signal) and fit. $C_{(1-x)}H_x$: x = 19%
Sample 12: ERD spectra (H signal) and fit. $C_{(1-x)}H_x$: x = 18%
Sample 13: ERD spectra (H signal) and fit. $C_{(1-x)}H_x$: x = 10%
Sample 14: ERD spectra (H signal) and fit. $C_{(1-x)}H_x$: x = 16%
Sample 15: ERD spectra (H signal) and fit. $C_{(1-x)}H_x$: x = 18%
Sample 16: ERD spectra (H signal) and fit. $C_{(1-x)}H_x$: x = 27%
Sample 17: ERD spectra (H signal) and fit. $C_{(1-x)}H_x$: x = 27%

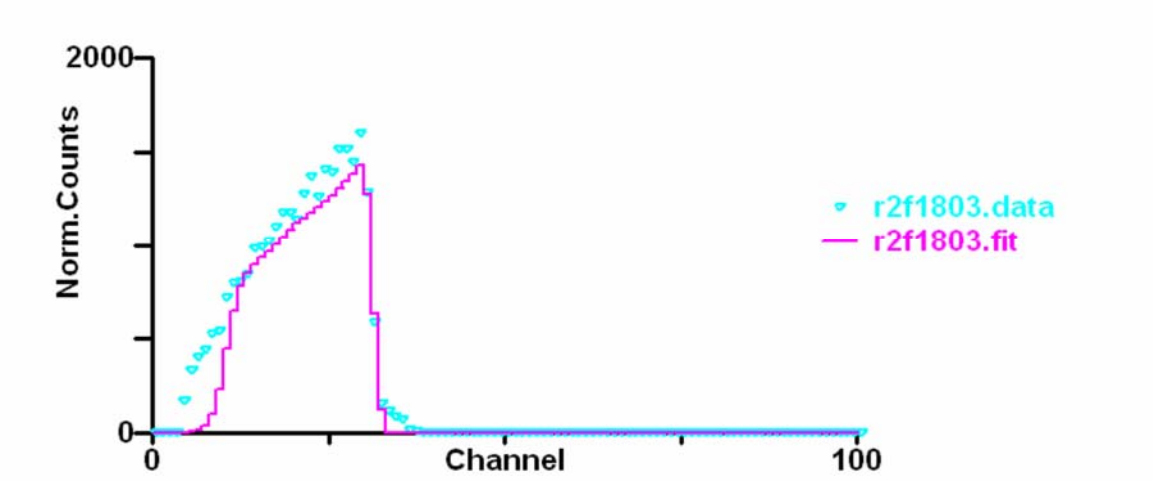

Sample 18: ERD spectra (H signal) and fit. $C_{(1-x)}H_x$: x = 30.4%

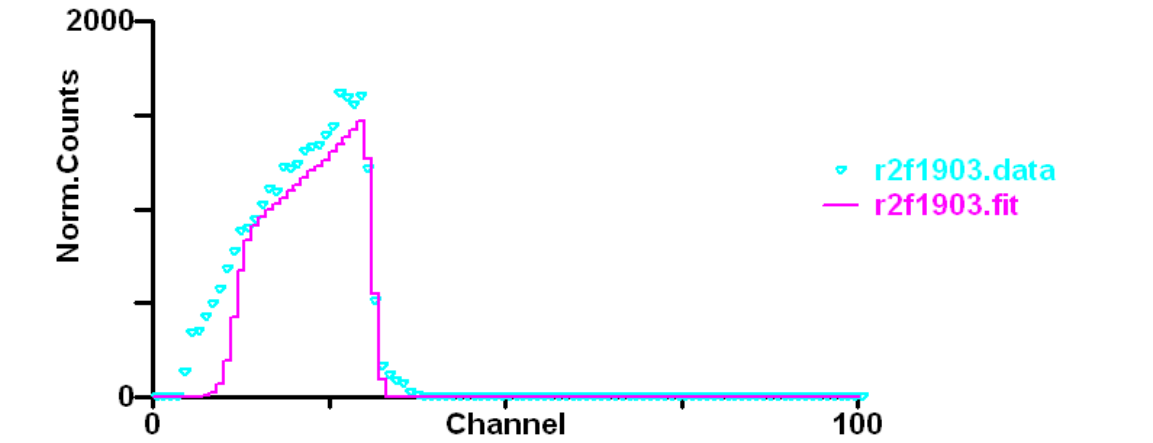

Sample 19: ERD spectra (H signal) and fit. $C_{(1-x)}H_x$: x = 32.4%

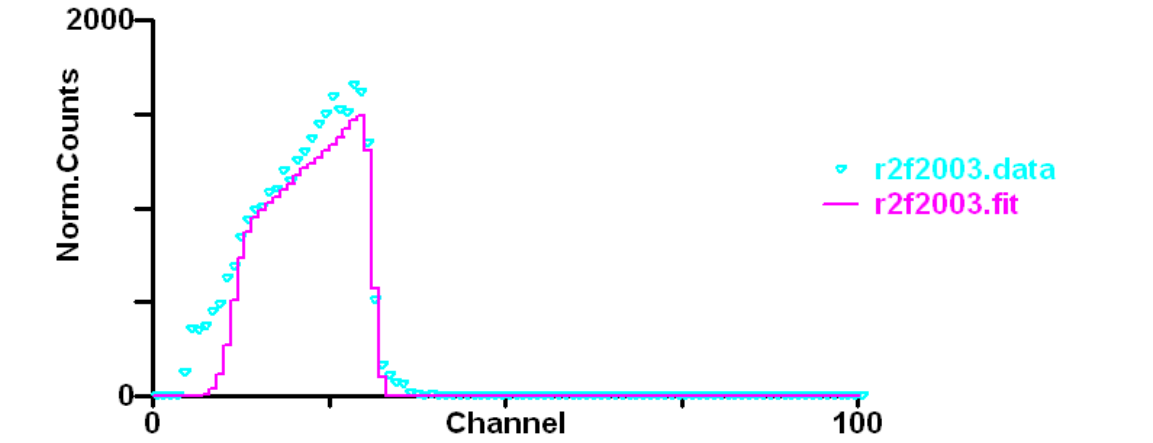

Sample 20: ERD spectra (H signal) and fit. $C_{(1-x)}H_x$: x = 37%

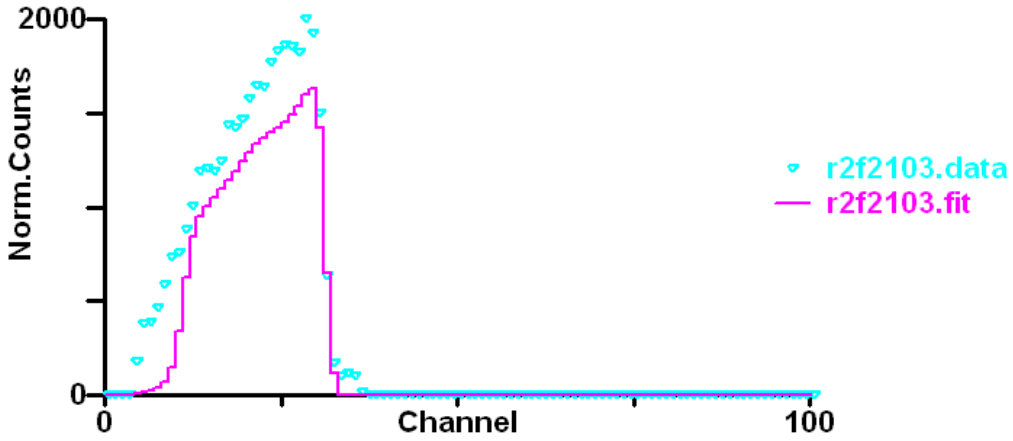

Sample 21: ERD spectra (H signal) and fit. $C_{(1-x)}H_x$: x = 32.1%

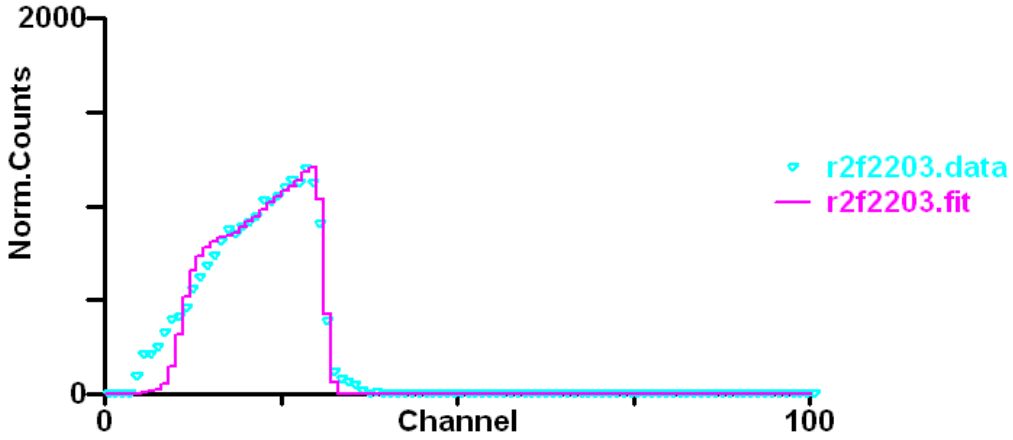

Sample 22: ERD spectra (H signal) and fit. $C_{(1-x)}H_x$: x = 28.8%

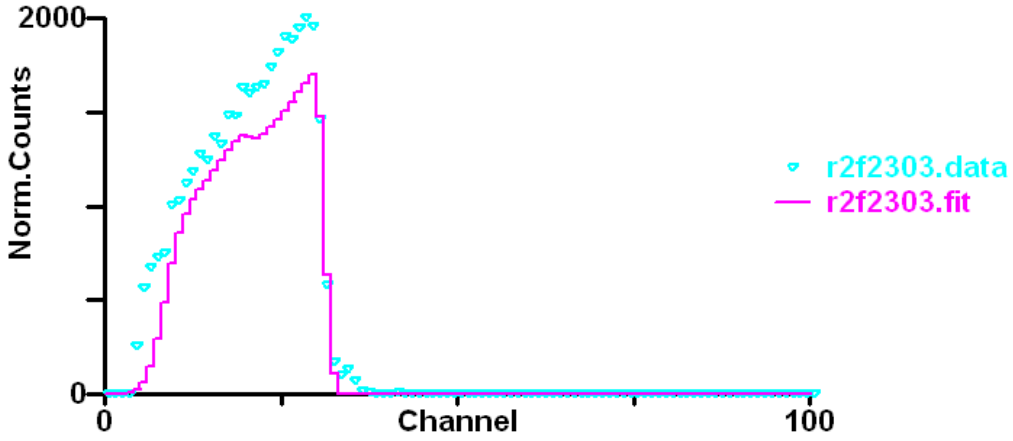

Sample 23: ERD spectra (H signal) and fit. $C_{(1-x)}H_x$: x = 32.1%

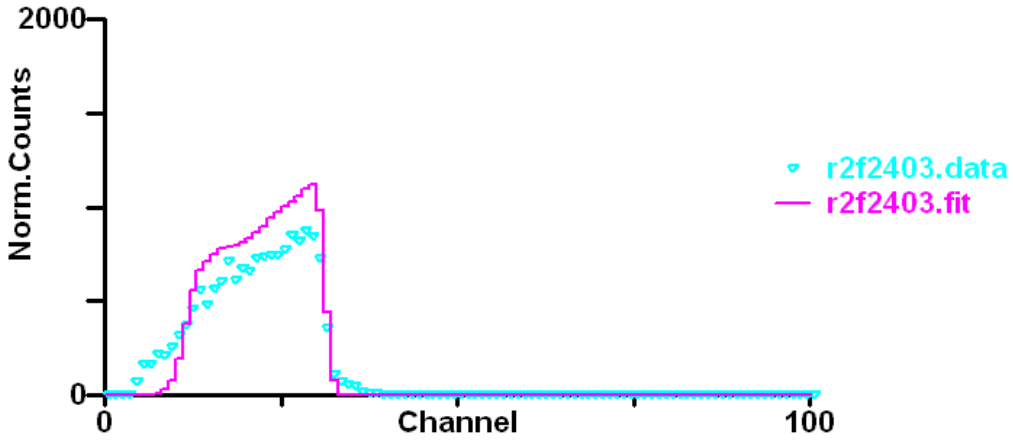

Sample 24: ERD spectra (H signal) and fit. $C_{(1-x)}H_x$: x = 19%
Sample 25: ERD spectra (H signal) and fit. $C_{(1-x)}H_x$: x = 1.4%
Sample 26: ERD spectra (H signal) and fit. $C_{(1-x)}H_x$: x = 1.4%
Sample 27: ERD spectra (H signal) and fit. $C_{(1-x)}H_x$: x = 1.8%
Sample 28: ERD spectra (H signal) and fit. $C_{(1-x)}H_x$: x = 29%
Sample 29: ERD spectra (H signal) and fit. $C_{(1-x)}H_x$: x = 28%
Sample 30: ERD spectra (H signal) and fit. $C_{(1-x)}H_x$: x = 30%
Sample 31: ERD spectra (H signal) and fit. $C_{(1-x)}H_x$: x = 25%
Sample 32: ERD spectra (H signal) and fit. $C_{(1-x)}H_x$: x = 2.1%

Sample 1
Sample 2
Sample 3
Sample 4
Sample 5
Sample 6
Sample 7
Sample 8
Sample 9
Sample 10
Sample 11
Sample 12
Sample 13
Sample 14
Sample 15
Sample 16
Sample 17

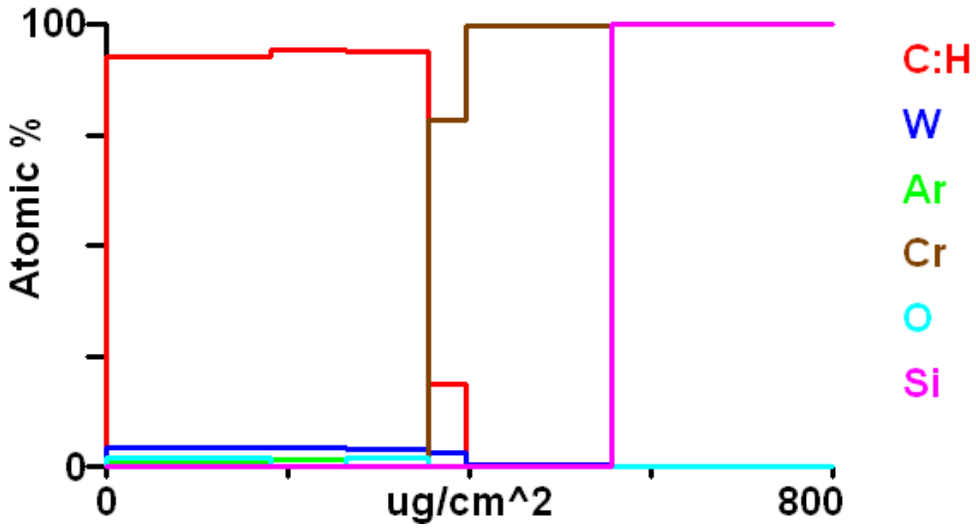

Sample 18

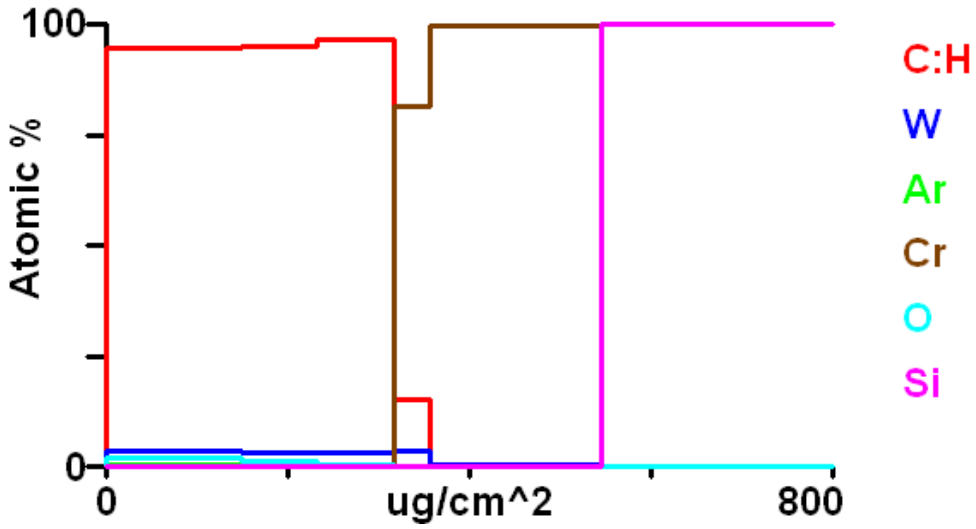

Sample 19

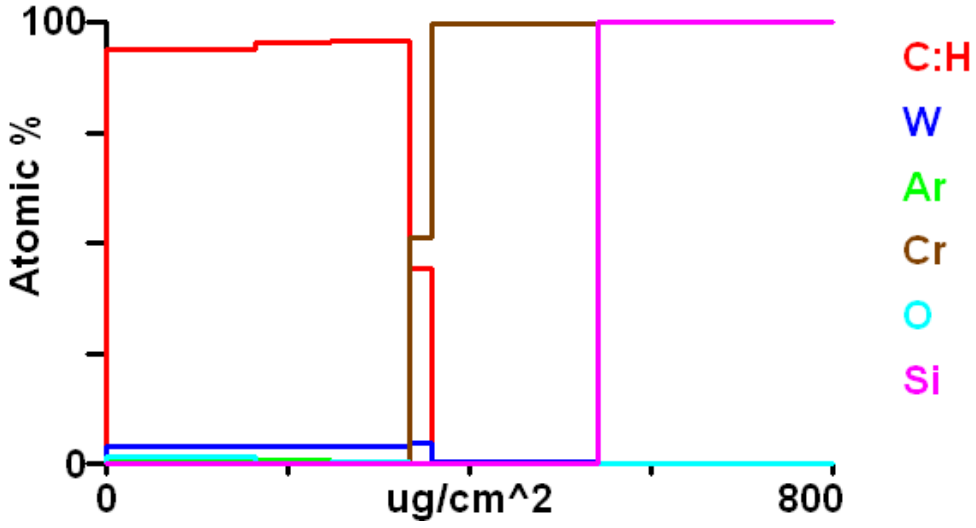

Sample 20

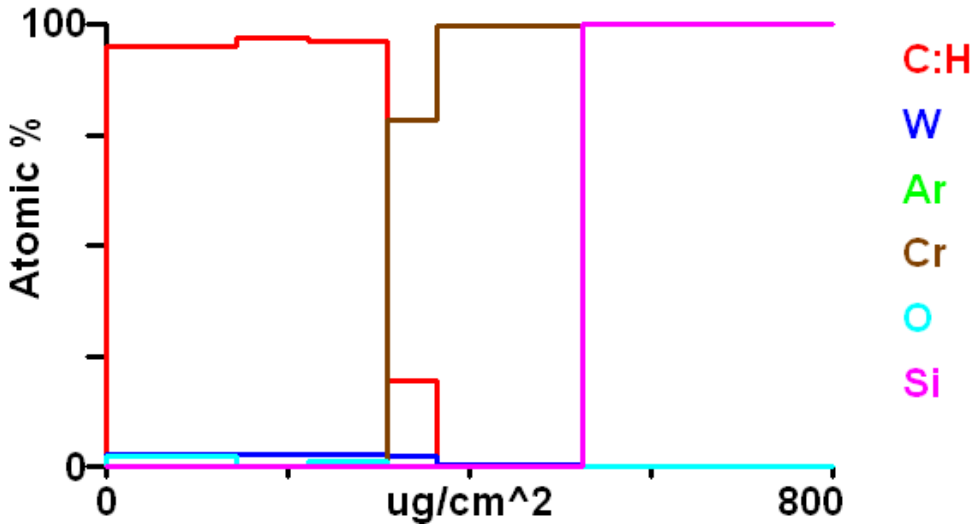

Sample 21

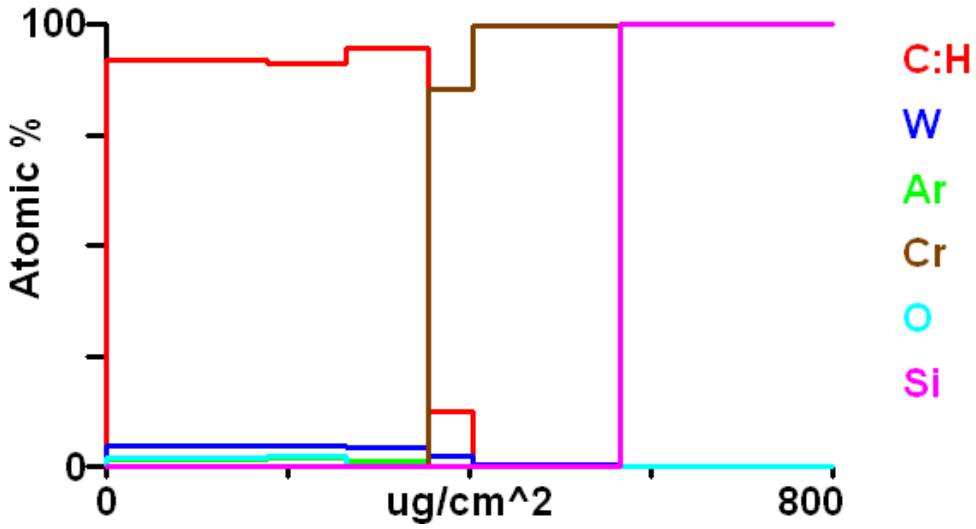

Sample 22

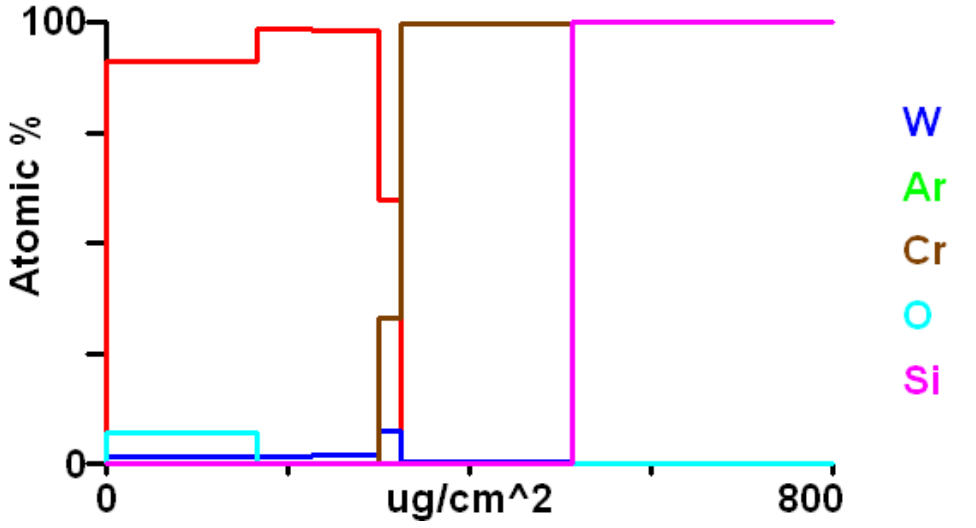

Sample 23

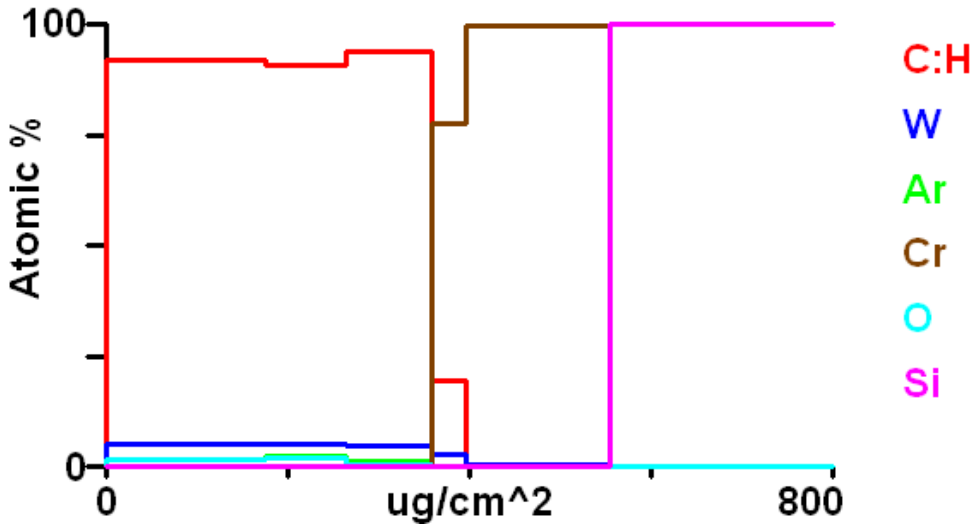

Sample 24
Sample 25
Sample 26
Sample 27
Sample 28
Sample 29
Sample 30
Sample 31
Sample 32

Reference

1. Boudreault, G.; Elliman, R.G.; Grötzschel, R.; Gujrathi, S.C., Jeynes, C.; Lennard, W.N.; Rauhala, E.; Sajavaara, T.; Timmers, H.; Wang, Y.Q.; et al. Round Robin: measurement of H implantation distributions in Si by elastic recoil detection. *Nucl. Instrum. Methods B* **2004**, *222*, 547–566.
2. Barradas, N.P.; Jeynes, C. Advanced physics and algorithms in the IBA DataFurnace. *Nucl. Instrum. Methods B* **2008**, *266*, 1875–1879, https://doi.org/10.1016/j.nimb.2007.10.044.
3. Abriola, D.; Barradas, N.P.; Bogdanović-Radović, I.; Chiari, M.; Gurbich, A.F.; Jeynes, C.; Kokkoris, M.; Mayer, M.; Ramos, A.R.; Shi, L.; et al. Development of a reference database for Ion Beam Analysis and future perspectives, *Nucl. Instrum. Methods B*, **2011**, *269* 2972–2978
4. Gurbich, A. Evaluated differential cross-sections for IBA. *Nucl. Instrum. Methods B* **2010**, *268*, 1703–1710, https://doi.org/10.1016/j.nimb.2010.02.011.
5. J. F. Ziegler, SRIM-2003. *Nucl. Instrum. Methods B* **2004**, *219*, 1027–1036
6. Wielopolski, L.; Gardner, R.P.; Prediction of the pulse-height spectral distortion caused by the peak pile-up effect. *Nucl. Instrum. Methods B* **1976**, *133*, 303–309
7. Molodtsov, S.L.; Gurbich, A.F. Simulation of the pulse pile-up effect on the pulse-height spectrum. *Nucl. Instrum. Methods B* **2009**, *267*, 3484–3487
8. Pascual-Izarra, C.; Barradas, N.P. Introducing routine pulse height defect corrections in IBA. *Nucl. Instrum. Methods B*, **2008**, *266*, 266–270
9. Barradas, N.P. Rutherford backscattering analysis of thin films and superlattices with roughness. *J. Phys. D: Appl. Phys.*, **2001**, *34*, 2109–2116
10. Simon, A.; Jeynes, C.; Webb, R.P.; Finnis, R.; Tabatabaian, Z.; Sellin, P.J.; Breese, M.B.H.; Fellows, D.F.; van den Broek, R.; and Gwilliam, R.M. The new Surrey ion beam analysis facility. *Nucl. Instrum. Methods B* **2004**, *219*, 405–409.
11. Grime, G.W.; and Dawson, M. Recent developments in data acquisition and processing on the Oxford scanning proton microprobe. *Nucl. Instrum. Methods B* **1995**, *104*, 107–113.
12. Blaauw, M.; Campbell, J.L.; Fazinić, S.; Jakšić, M.; Orlic, I.; and van Espen, P. The 2000 IAEA intercomparison of PIXE spectrum analysis software. *Nucl. Instrum. Methods B* **2002**, 189, 113–122.
13. Jeynes, C., Barradas, N.P.; Marriott, P.K.; Boudreault, G.; Jenkin, M.; Wendler, E.; and Webb, R.P. Elemental thin film depth profiles by ion beam analysis using simulated annealing-a new tool. *J. Phys. D* **2003**, *36*, R97.
14. Boudreault, G.; Jeynes, C.; Wendler, E.; Nejim, A.; Webb, R.P.; and Wätjen, U. Accurate RBS measurement of ion implant doses in silicon. *Surf. Interface Anal.* **2002**, *33*, 478–486.

15. Barradas, N.P.; Arstila, K.; Battistig, G.; Bianconi, M.; Dytlewski, N.; Jeynes, C.; Kótai, E.; Lulli, G.; Mayer, M.; Rauhala, E.; et al. Summary of "IAEA intercomparison of IBA software". *Nucl. Instrum. Methods B* **2008**, *266*, 1338–1342.
16. Pascual-Izarra, C.; Barradas, N.P.; Reis, M.A.; Jeynes, C.; Menu, M.; Lavedrine, B.; Ezrati, J.J. and Röhrs, S. Towards truly simultaneous PIXE and RBS analysis of layered objects in cultural heritage. *Nucl. Instrum. Methods B* **2007**, *261* 426–429.